EAI Endorsed Transactions
on Energy Web
Research Article EAI.EU

Analysis of optimal scheduling and energy-saving measures for shipyard microgrid based on IMOPSO algorithm

Weipeng Li[1], Jun Du[1,*], Jiao Wang[1], Tong Fu[1], Sitong Zhu[1]

[1]School of Energy and Power, Jiangsu University of Science and Technology, Zhenjiang 212100, China

Abstract

INTRODUCTION: This research study presents the development of a microgrid system specifically designed for a shipyard environment based on the energy consumption characteristics of major shipyard equipment.
OBJECTIVES: The algorithm simultaneously optimizes three different objectives as follows: (1) economic cost; (2) carbon emission; and (3) power fluctuation (stability).
METHODS: To accomplish the objective of creating an optimal microgrid configuration, the IMOPSO was used to solve the microgrid model.
RESULTS: Results indicate that there are considerable trade-offs between economic cost versus carbon emission and between economic cost versus power fluctuation, which require optimally balanced approaches in order to meet all the different objectives. Among various energy-saving measures, the adoption of the dehumidification system with heat recovery wheel proves especially effective in reducing power consumption, economic cost and carbon emission.
CONCLUSION: Pareto front analysis reveals that the weak emission-fluctuation conflict creates an opportunity to effectively balance the critical cost-emission trade-off for obtaining superior solutions. Equipment energy-saving measures, particularly the dehumidification with heat recovery and hybrid welding, significantly improve the microgrid's economic and environmental performance.

Keywords: Microgrid Optimization, MOPSO Algorithm, Shipyard Energy Consumption, Energy-saving Measures, Multi-objective Trade-offs

Received on 23 May 2026, accepted on 07 July 2026, published on 21 July 2026

doi: 10.4108/ew.13144

1. Introduction

Under China's "dual carbon" goals, improving energy efficiency is vital for manufacturing transformation. Shipyards, as energy-intensive sites, are characterized by concentrated loads and significant power fluctuations. Microgrid technology offers a promising solution by integrating distributed energy resources and enabling optimized load management. This study develops equipment-level load models and investigates microgrid scheduling strategies to enhance energy management in shipyards.

Numerous scholars have extensively investigated the optimal scheduling of microgrids. Xue et al. [1] analyzed the current status of economic dispatch research for microgrids both domestically and internationally from

*Corresponding author. Email: dujun9988@163.com

multiple perspectives, identified existing challenges, and provided a summary and outlook. Li and Xu [2] developed an optimal system-wide strategy for coordinated energy dispatch in a microgrid system with multiple energy under both operational modes. Guan et al. [3] used an modified PSO algorithm to address the grid-connected microgrids' multi-objective scheduling problem. Ma et al. [4] introduced a bird swarm algorithm integrated with an self-adaptive levy flight strategy. Nguyen et al. [5] introduced a new sparrow search algorithm to improve microgrid scheduling and management. Tiwari et al. [6] solved the problem of integrating a BES system into the MG by applying the wild geese algorithm. Dai et al. [7] presented a shared energy storage framework of multi-microgrid, aiming to determine virtual storage capacity dynamically during operation, to reduce the physical energy storage capacity requirements. He et al. [8] proposed an advanced multi-objective war strategy optimization (MOWSO) algorithm to tackle intricate multi-objective dispatch issues in microgrids. Wu et al. [9] applied a hierarchical control scheme for microgrids and utilized an enhanced PSO algorithm to optimize multiple objectives in tertiary control. Wang et al. [10] presented a bi-level scheduling model applied to a shipboard hybrid microgrid integrating electricity, gas, and heat, and solved it using the MOPSO algorithm. Ouammi et al. [11] developed an energy management framework based on MPC integrated with a microgrid, aiming at optimal regulation of environmental conditions and crop production while accounting for renewable energy variability, storage dynamics, and climate uncertainties. Ghadi-Sahebi and Ebrahimi [12] proposed energy management strategies for a grid-connected microgrid equipped with distributed generators and electric vehicles by creating a multi-objective optimization framework that incorporates uncertainties, and showed that their modified MOPSO algorithm is effective.

In order to study microgrid systems in shipyards, it is necessary to research relevant literature on energy-consuming equipment. There is a considerable amount of work done in regard to energy efficient design of all equipment types and energy utilization strategies for all types of energy utilizing equipment. Cheng et al. [13] presented air compressor design principles, operational characteristics and the energy conservation solutions being utilized in the industrial sector. Hu et al. [14] proposed a pre-cooling system for air compressors and confirmed its feasibility. Hummel et al. [15] proposed a compressed air electrical ratio (CAER) as an important means of determining power consumption of air compressors, and provided an analysis of fixed-speed vs variable-speed compressors, as well as determining the important factors affecting CAER values. Liu et al. [16] examined the influence of parameters in the welding process on the energy performance of laser–GTA hybrid welding processes. Mahrle et al. [17] studied how the laser beam interacts with the plasma arc, demonstrating significant improvements in arc stability and welding performance. Chen et al. [18] presented a pre-cooling desiccant-wheel AC system, suitable for challenging environments. Srivastava et al. [19] reviewed the development of thermoelectric dehumidifiers, discussed their current status, and suggested future directions. Costa et al. [20] investigated a nozzle–diffuser method inspired by the Foehn effect for dehumidification, showing nearly tenfold energy savings compared to conventional mechanical refrigeration dehumidifiers. Qu et al. [21] introduced a crane energy consumption evaluation method that considers the working cycle of the service period, analyzing typical service working mode and clarifying the working cycle process of the mechanism. Kłodawski et al. [22] developed a simulation-based approach to evaluate crane energy consumption in intermodal terminals, highlighting that loading strategies significantly affect energy efficiency, costs, and environmental impact. Fei et al. [23] established a power balance equation based on the energy flow in bridge cranes, providing theoretical support for crane energy consumption evaluation. Jones et al. [24] examined laser cutting, welding, and cleaning to evaluate overall energy use and carbon footprint in laser-based manufacturing.

This paper proposes a tri-objective microgrid dispatch model for shipyards, incorporating equipment energy consumption models as the load profile and is optimized using the IMOPSO algorithm. The paper proceeds as follows: Section 2, shipyard microgrid model is formulated. Section 3, IMOPSO algorithm is detailed. Section 4, optimization results are presented. And section 5 presents the conclusion of the study.

2. Modeling of Shipyard Microgrid

The paper focuses on a microgrid designed for shipyards, as shown in Fig. 1. Following discussions with the project team's engineers and further research, it has been established that these five categories of devices account for the largest proportion of energy consumption at the shipyard. Therefore, we decided to construct the shipyard microgrid system as shown in Fig. 1. On the source side, the system includes PV (photovoltaic), WT (wind turbines), DG (diesel generators), MT (micro turbines), ESS (energy storage systems). Through the connection lines, the main grid can trade with the microgrid in both directions. The load side comprises five major energy-consuming devices used in shipyards, along with other auxiliary loads (represented as fixed values and therefore not shown in Fig. 1). The five devices include air compressors, welding machines, cranes, dehumidifiers, and cutting machines.

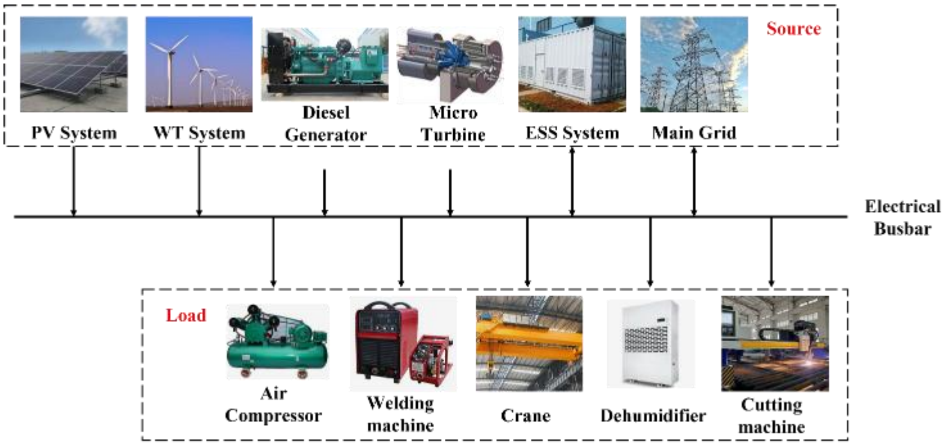

Figure 1. Microgrid system diagram for shipyards

2.1. Distributed Generation Model

(1) DG.

$$\begin{cases} C_{DG.OM}(t) = K_{DG.OM} P_{DG}(t) \\ C_{DG.F}(t) = \alpha P_{DG}^2(t) + \beta P_{DG}(t) + \gamma \end{cases} \tag{1}$$

$C_{DG.OM}(t)$, $C_{DG.F}(t)$ are DG's O&M (operation and maintenance) cost and fuel cost at time t. $P_{DG}(t)$ represents the output power of DG. $K_{DG.OM}$ is the DG O&M cost coefficient. α, β, γ are DG-related coefficients, with values α = 0.00011, β = 0.1801, γ = 6.

(2) MT

MT's fuel cost ($C_{MT.F}$), O&M cost ($C_{MT.OM}$) are calculated as follows:

$$\eta_{MT}(t) = 0.0753[\frac{P_{MT}(t)}{65}]^3 - 0.3095[\frac{P_{MT}(t)}{65}]^2 + 0.4174\frac{P_{MT}(t)}{65} + 0.1068 \tag{2}$$

$$\begin{cases} C_{MT.OM}(t) = K_{MT.OM} P_{MT}(t) \\ C_{MT.F}(t) = \dfrac{C}{LHV} \dfrac{P_{MT}(t)}{\eta_{MT}(t)} \end{cases} \tag{3}$$

$P_{MT}(t)$, $\eta_{MT}(t)$ represent the output power and efficiency of MT, respectively. $K_{MT.OM}$ is MT's O&M cost coefficient. C and LHV represent natural gas price and lower heating value, respectively.

(3) ESS

$$SOC(t) = \begin{cases} SOC(t-1) - \eta_{cha} P_{ESS}(t), P_{ESS}(t) \le 0 \\ SOC(t-1) - \dfrac{P_{ESS}(t)}{\eta_{dis}}, \quad P_{ESS}(t) > 0 \end{cases} \tag{4}$$

SOC(t) is the remaining capacity of ESS at time t. η_{dis}, η_{cha} are the efficiency of the discharging and charging processes, with values η_{dis} = η_{cha} = 0.9. The charge/discharge efficiency of the ESS are based on the typical charge/discharge efficiency of lithium-ion battery (0.85-0.95). $P_{ESS}(t)$ is the ESS output power, positive during discharge and negative during charge.

2.2. Objective Function and Constrains

$$\min F = \min(f_1, f_2, f_3) \tag{5}$$

f_1, f_2 and f_3 denote the economic cost, carbon emission and power fluctuation, respectively. The three objective functions are set to take into account economic, environmental and stability considerations.

(1) Economic cost.

$$\min f_1 = \sum_{t=1}^{T} C_s(t), \quad s = WT/PV/DG/MT/ESS/GRID \tag{6}$$

$C_i(t)$ represents the costs of the six power units (i=WT, PV, DG, MT, ESS, GRID). $C_{WT}(t)$, $C_{PV}(t)$ and $C_{ESS}(t)$ comprise the O&M cost (C_{OM}) and depreciation cost (C_{DP}). $C_{DG}(t)$ and $C_{MT}(t)$ comprise the C_{OM}, C_{DP} and fuel cost (C_F). $C_{GRID}(t)$ includes the electricity purchase cost $C_{purchase}(t)$ and electricity selling revenue $C_{sold}(t)$.

$$\begin{cases} C_{j.OM}(t) = K_{j.OM}\left|P_j(t)\right|, \\ C_{j.DP}(t) = \dfrac{c_j}{8760 f_j} \dfrac{r(1+r)^l}{(1+r)^l - 1}\left|P_j(t)\right|, \end{cases} \quad j = WT/PV/ESS/DG/MT \tag{7}$$

$K_{j.OM}$, $P_j(t)$, c_j, f_j represent the O&M cost coefficient, output power at time t, installation cost, and capacity factor of source j, respectively. r denotes the annual interest rate. l is the service lifetime (in years).

$$\begin{cases} C_{GRID}(t) = C_{buy}(t) - C_{sell}(t) \\ C_{buy}(t) = c_{buy}(t)P_{buy}(t) \\ C_{sell}(t) = c_{sell}(t)P_{sell}(t) \end{cases} \tag{8}$$

$c_{purchase}(t)$, $c_{sold}(t)$ are the electricity prices for purchase and sale, and $P_{sold}(t)$, $P_{purchase}(t)$ are the corresponding sold and purchased powers.

(2) Carbon emission

$$\min f_2 = \sum_{t=1}^{T}\left[e_1P_{buy}(t) + e_2P_{DG}(t) + e_3P_{MT}(t)\right] \tag{9}$$

e_1, e_2, e_3 are the carbon dioxide emission coefficient corresponding to main grid power purchases, DG, MT, respectively.

(3) Power fluctuation (stability)

$$\min f_3 = \frac{\sqrt{\sum_{t=2}^{N}[P_{GRID}(t) - P_{GRID}(t-1)]^2}}{N} \tag{10}$$

$P_{GRID}(t)$ indicates the exchanged power at time t (positive for import, negative for export). N is the daily number of hours.

(4) Constraints

1) Energy balance constraint

$$\begin{aligned} &P_{PV}(t) + P_{WT}(t) + P_{DG}(t) + P_{MT}(t) \\ &+P_{ESS}(t) + P_{GRID}(t) = P_{LOAD}(t) \end{aligned} \tag{11}$$

$P_{LOAD}(t)$ denotes the load at time t.

2) Operational constraints

$$\begin{aligned} &\begin{cases} SOC_{\min} \le SOC(t) \le SOC_{\max}, \\ P_{g,\min} \le P_g(t) \le P_{g,\max}, \\ |P_k(t+1) - P_k(t)| \le r_k, \end{cases} \\ &g = ESS/DG/MT/GRID \\ &k = DG/MT \end{aligned} \tag{12}$$

SOC_{min}, SOC_{max} indicate the SOC limits. $P_{g,max}$, $P_{g,min}$ are the upper and lower power boundaries of power unit g. r_k denotes the distributed generator k's ramp limit (200 kW/h).

2.3. Energy-consumption Modeling of Equipment

(1) Air compressor

The air compressor is modeled as an isentropic process based on thermodynamic principles, with its compression work given by Eq. (13).

$$W_{comp} = \dot{m}\cdot\frac{k}{k-1}\cdot R\cdot T_{in}\cdot(r^{\frac{k-1}{k}} - 1)\Big/\eta_{comp} \tag{13}$$

m, k, R, T_{in}, r, η_{comp} denotes the air mass flow, specific heat ratio, gas constant, inlet air temperature, compression ratio, and isentropic efficiency, respectively.

The compression energy consumption per unit mass of refrigerant W_{cold_unit} is derived from Eq. (5) in Ref. [14].

(2) Welding machine

The welding machine is modeled based on arc and laser welding technologies, with its energy consumption E for a specific task given by Eq. (1) of Ref. [16].

(3) Dehumidifier

Under the assumption that heating energy equals electricity consumption, the energy consumption for regeneration of the desiccant wheel dehumidification with and without heat recovery (denoted as Q_r and Q'_r, respectively) are as follows.

$$E_h = Q_r = m_r \cdot c_r \cdot (T_h - T_g) \tag{14}$$

$$E_h = Q_r^{'} = m_r \cdot c_r \cdot (T_h - T_a) \tag{15}$$

m_r, c_r, T_h, T_g and T_a indicate the mass flow, specific heat, inlet/outlet temperatures of the regeneration air, and ambient temperature.

The cooling equipment energy consumption (E_c) is calculated as follows:

$$E_c = \frac{Q_c}{COP_c} \tag{16}$$

Q_c is the cooling load handled by the cooling equipment under pre-cooling conditions. COP_c indicates the cooling equipment's coefficient of performance.

The total energy consumption E is given in Eq. (17).

$$E = E_h + E_c + E_{p/f} \tag{17}$$

$E_{p/f}$ is the electrical energy consumed by pumps, fans, and motors.

(4) Crane

The energy consumption model for the bridge crane is adopted from Eqs. (4), (9), and (10) in Ref. [21].

(5) Cutting machine

The energy consumption model for the cutting machine, characterizing the inverse relationship between the specific energy consumption (SEC) and processing rate (PR), is adopted directly from Eq. (1) in Ref. [24].

3. IMOPSO Algorithm

The IMOPSO algorithm combines the non-dominated sorting strategy with the external archive maintenance strategy based on adaptive grid.

Eq. (18) describe the updates of position and velocity:

$$\begin{cases} x_{id}^{t+1} = x_{id}^{t} + v_{id}^{t+1} \\ v_{id}^{t+1} = \omega v_{id}^{t} + \\ c_1r_1\left(p_{id,\text{pbest}}^{t} - x_{id}^{t}\right) + c_2r_2\left(p_{d,\text{gbest}}^{t} - x_{id}^{t}\right) \end{cases} \tag{18}$$

x_{id}^t, v_{id}^t are particle i's position and velocity in dimension d at iteration t. ω denotes the inertia weight. c_1, c_2 represent cognitive and social learning factors. r_1, r_2 represent random numbers. $p_{id,pbest}^t$ and $p_{d,gbest}^t$ denote the best positions of personal and global in dimension d.

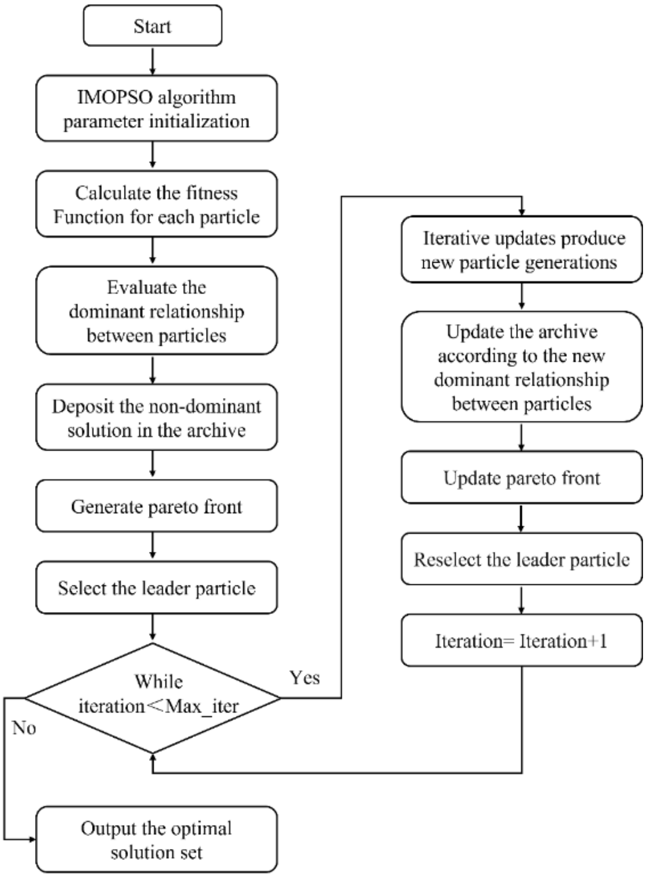

Figure 2. IMOPSO algorithm flowchart

The IMOPSO algorithm introduces adaptive parameter adjustment and mutation operators to enhance both global exploration and local exploitation. Fig. 2 shows the IMOPSO algorithm flowchart.

Equations for inertia weight and learning factors employed in this work are presented as follows (see reference[3]):

$$w = w_{\max} - (w_{\max} - w_{\min})\frac{t}{t_{\max}} \tag{19}$$

t represents the present iteration. t_{max} represents the maximum iterations. ω_{max}, ω_{min} represent the initial and final inertia weights, respectively. In this paper, the parameter values are set as $t_{max} = 200$, and $\omega_{max} = 0.9$, $\omega_{min} = 0.4$.

$$c_1 = (c_{1f} - c_{1i})\frac{t}{t_{\max}} + c_{1i} \tag{20}$$

$$c_2 = (c_{2f} - c_{2i})\frac{t}{t_{\max}} + c_{2i} \tag{21}$$

The initial and final cognitive (c_{1i}, c_{1f}), social (c_{2i}, c_{2f}) learning coefficients are set to 2.5, 0.5, 0.5, and 2.5, respectively.

4. Simulation Studies

4.1. Simulation Setting

A case of a shipyard in Shanghai is conducted. The simulation is performed using MATLAB R2023b. By establishing energy consumption models for the main energy-consuming equipment in the shipyard, the hourly power demand of each device is calculated and aggregated to simulate the shipyard's total hourly power demand. For a typical day, the shipyard's power demand was obtained based on the operational schedule and models of the main energy-consuming equipment.

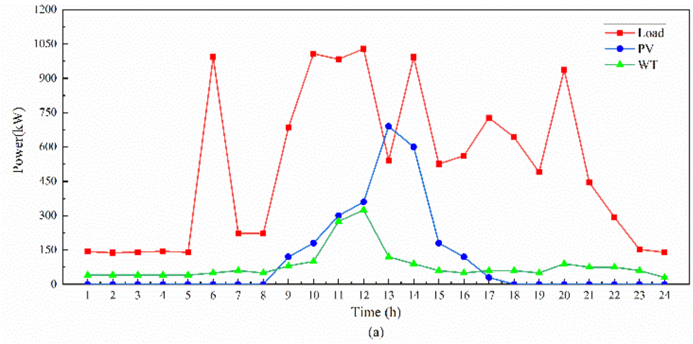

Figure 3. Predicted WT, PV, and Load Profiles

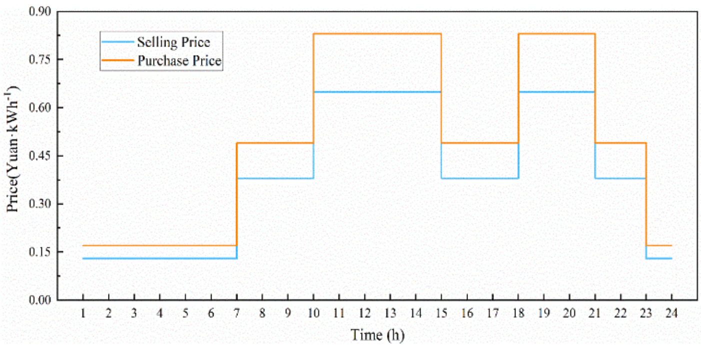

Figure 4. Real-time electricity price curve for one day

Fig. 3 depicts the predicted WT and PV outputs along with the load demand curve, the load profile of a typical shipyard day exhibits the following characteristics: Power demand peaks at 6:00 during equipment startup, rises to a second peak by noon, then drops at 13:00 during lunch. A third peak occurs post-break, followed by a general decline despite an evening surge at 20:00 from an emergency task. Fig. 4 provides the one-day real-time electricity price profile.

Tables 1-4 summarize the key parameters of the system components:

Table 1 shows the parameters of distributed energy resources (DERs).

Table 2 shows the carbon dioxide emission factors of DERs.

Table 3 shows the ESS characteristics.

Table 4 shows the power limits of each DER.

Table 1. Parameters of DERs

Type	Operating cost (Yuan/kWh)	Depreciation period (Year)	Installation cost(10^4 Yuan/kWh)	Capacity factor (%)
PV	0	20	6.65	29.34
WT	0	10	2.375	22.13
DG	0.128	10	4.275	36.73
MT	0.0293	15	1.609	54.99

Table 2. Carbon dioxide emission factors of DERs

Type	Carbon dioxide emission factors (g/kWh)				
	PV	WT	DG	MT	Grid
CO_2	0	0	680	724	889

Table 3. Characteristics of ESS

Parameter	Value	Parameter	Value
Maximum capacity (kWh)	1000	Installation cost (Ten Thousand Yuan/kWh)	0.087
Minimum capacity (kWh)	100	Capacity factor (%)	29.34
Power upper limit(kW)	400	Depreciation period (Year)	10
Power lower limit(kW)	-400	Operating cost (Yuan/kWh)	0.026

Table 4. The power limits of each DER

Parameter	DG	MT	Grid
Power upper limit(kW)	400	400	1000
Power lower limit(kW)	40	40	-1000

4.2. Case Analysis

4.2.1. Comparison of Different System Configurations

To evaluate whether the proposed microgrid configuration is reasonable, the paper compared three alternative scenarios: (1) without PV/WT; (2) without DG/MT; (3) without ESS. For each configuration, the IMOPSO algorithm was independently executed 50 times to account for algorithmic randomness. The distributions of economic cost, carbon emission, and stability are presented as boxplots, as shown in Fig.5.

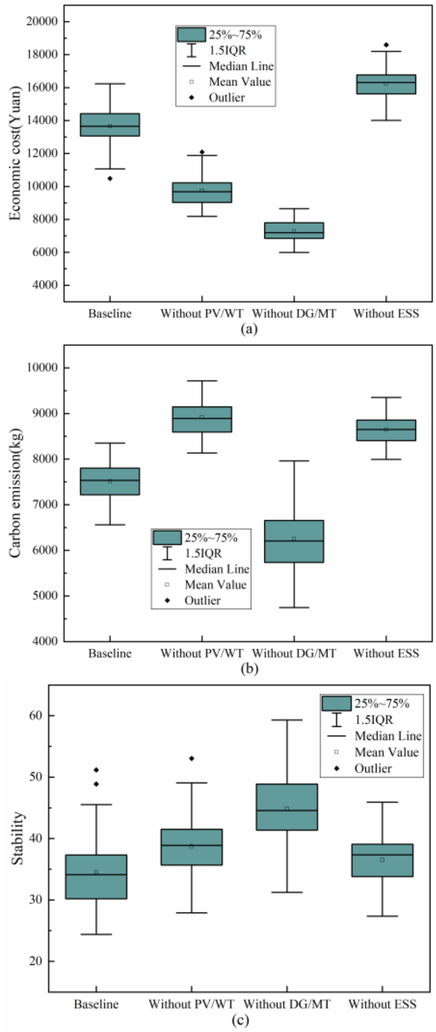

Figure 5. Boxplots of objective function comparison across different configurations. (a) economic cost; (b) carbon emission; (c) stability

The results indicate that although the baseline system (including all DERs) is not the minimum-cost configuration, it demonstrates the lowest power fluctuation and the second-lowest carbon emission. Removing PV/WT leads to the highest carbon emissions of any configuration while using the lowest-cost configuration (without

DG/MT) results in higher levels of power fluctuation compared to all other configurations. Thus, the baseline system represents a favourable balance between all three objectives (economic cost, carbon emission, and stability) through an acceptable and deliberate method of configuration selection.

4.2.2. Optimization Results

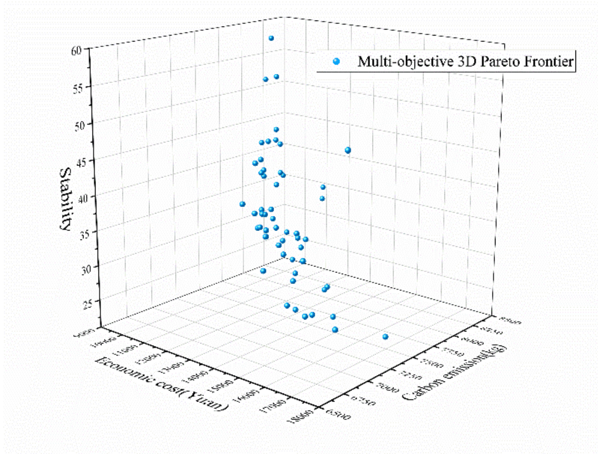

Figure 6. 3D pareto front

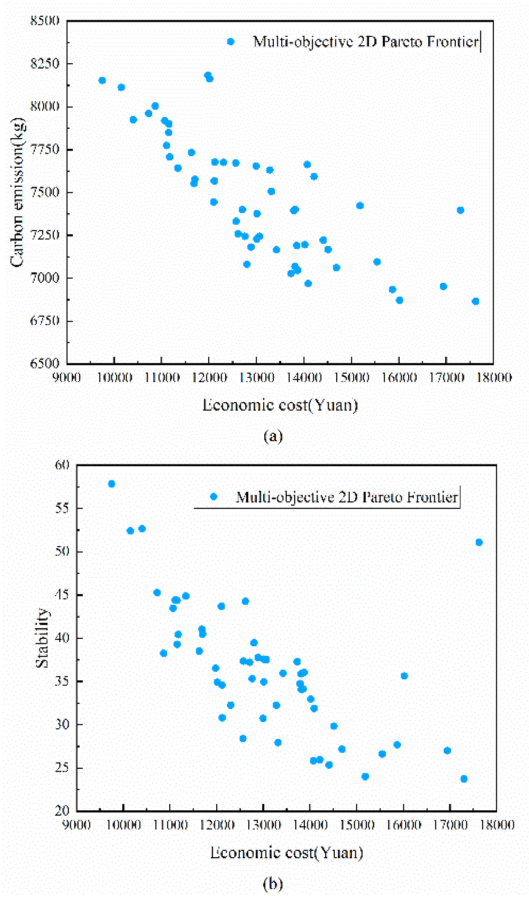

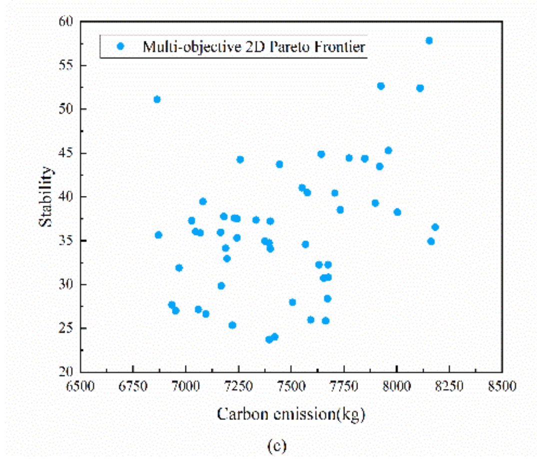

Figure 7. 2D pareto fronts

The optimization procedure was repeated a total of 50 times, and among those runs, the one that produced the smoothest Pareto front was selected. Fig. 6 and 7 illustrate the results. Fig. 6 presents the distribution of Pareto values as arranged in three-dimensional objective space by yielding a contiguous surface. Fig. 7 demonstrates that the Pareto fronts are generally smoother for the cost-emission and the cost-fluctuation performance measures indicating better established trade-offs, while the much more dispersed front for emission-fluctuation performances implies there is a weaker conflict. Since there is a low level of conflict between emission and fluctuation, an effective compromise can be made to optimise the cost and emission objectives together to create the best overall solution possible. The Pareto relationships above demonstrate that reducing economic cost usually comes at the expense of carbon emission and power fluctuation.

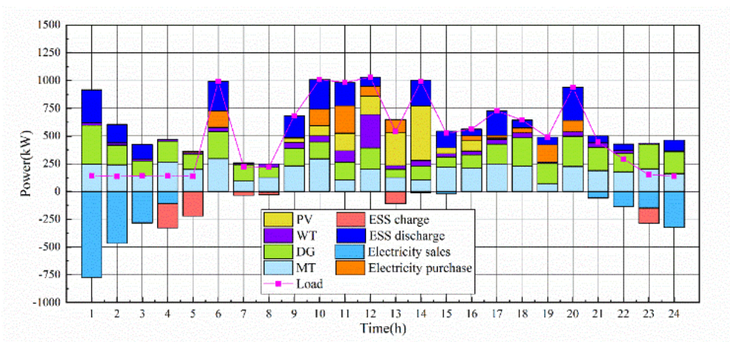

Figure 8. Optimal scheduling diagram for the microgrid

Fig. 8 presents the result. During the low-load timeframes of 1:00-5:00 and 22:00-24:00, the distributed generation systems provide energy for the loads and send surplus electricity back to the main grid while charging ESS with the remaining excess energy. At 6:00 there is a dramatic increase in load because of the beginning of the workday and loads at 8:00-11:00 steadily increase. At this point, the dispatch of all resources (distributed generation, ESS, and the main grid) has been achieved. At 12:00-14:00 WT and PV systems provide a high level of electricity. This indicates that the system is effectively using renewable energy for energy production, reducing the dependence of the microgrid on fossil fuels. At 15:00-21:00 the cost of storing energy in the ESS is lower than the cost of electricity from the main grid, so the ESS is used significantly during this timeframe to help meet the load while also using DG and MT; The grid energy plays a smaller role in the energy production process.

4.2.3. Impact of energy-saving Measures on Optimal Dispatch

Based on the 24-hour predicted PV/WT outputs and load profiles presented earlier, Fig. 9 compares the impacts of omitting specific energy-saving measures on total power, economic cost, and carbon emission against the baseline system incorporating all energy-saving measures, which is the same baseline system defined above. In each comparative system, only one specific measure is removed while all other measures remain enabled. The comparative systems include: Sys. 1 (air compressor without pre-cooling), Sys. 2 (GTA-only welding), Sys. 3 (laser-only welding), and Sys. 4 (dehumidification without heat recovery).

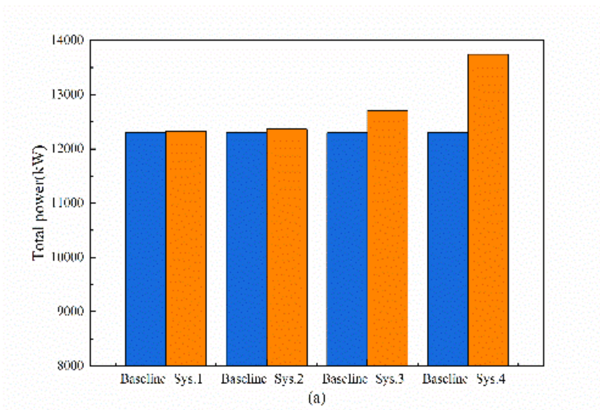

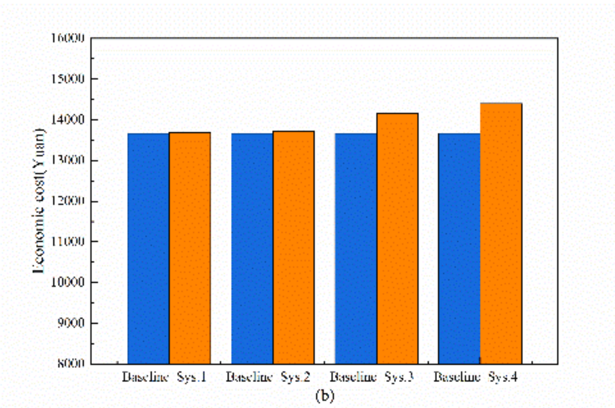

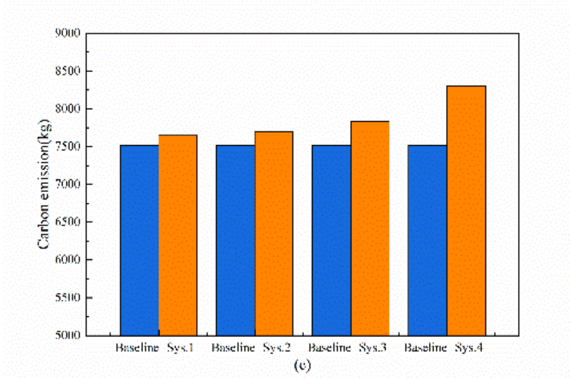

Figure 9. Comparison of system metrics with and without energy-saving measures. (a) total power; (b) economic cost; (c) carbon emission

The baseline system yields a total power consumption of 12,296.46 kW, an economic cost of 13,666.65 Yuan, and carbon emissions of 7,516.31 kg. The results of the comparative systems are summarized in Table 5.

Table 5. The results of the comparative systems

Systems	Total power/kW	Economic cost/Yuan	Carbon emission/kg
Sys.1	12,327.43 (+0.25%)	13,683.53 (+0.12%)	7,647.93 (+1.75%)
Sys.2	12,363.78 (+0.55%)	13,709.52 (+0.31%)	7,694.27 (+2.37%)
Sys.3	12,712.30 (+3.38%)	14,161.52 (+3.62%)	7,833.22 (+4.22%)
Sys.4	13,743.66 (+11.78%)	14,399.69 (+5.36%)	8,301.14 (+10.44%)

The results show that, while all measures impact system performance, the heat recovery desiccant wheel system notably reduces power, cost, and emissions due to high dehumidification needs in shipyards. In contrast, the welding method has a smaller impact, yet the poor performance of laser-only welding underscores the advantage of hybrid approaches. The pre-cooling module also proves effective in improving compressor efficiency.

4.2.4. Comparison of IMOPSO and MOPSO

Table 6 presents the algorithms' parameters. IMOPSO and MOPSO share the same basic parameters (population size, repository size, maximum iterations, and selection pressure), ensuring a fair comparison. The inertia weight and learning coefficient for IMOPSO have been described in Chapter 3.

Table 6. Parameters of the algorithms

Algorithm	Parameters	
MOPSO	Population size=100	Cognitive learning coefficient=2
	Maximum iterations=200	Social learning coefficient=2
	Repository size=100	Leader selection pressure=2
	Inertia weight=0.6	Deletion selection pressure=2
IMOPSO	Mutation rate=0.1	

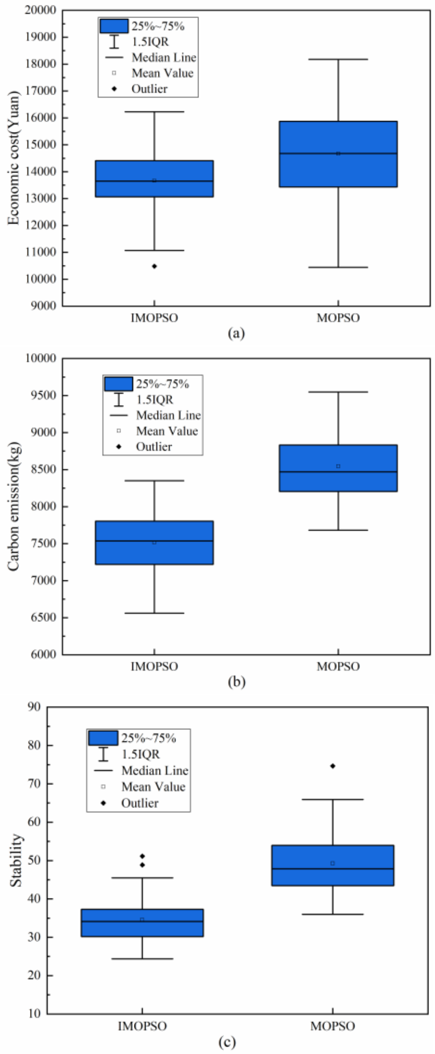

Figure 10. Boxplots comparison of the two algorithms across all objectives. (a) economic cost; (b) carbon emission; (c) stability

A comparison of the results achieved by both IMOPSO and MOPSO used the same evaluation methodology displayed in a series of boxplots (see Fig. 10). Both algorithms were executed a total of 50 times to generate the data for generating the boxplots used for each of the three objective functions. The boxplots illustrate that IMOPSO consistently produced lower objective values for all three objectives than did MOPSO, thus confirming that IMOPSO performed better than MOPSO overall. Therefore, it was determined that IMOPSO was to be used in this research project.

5. Conclusion

This study presents the study's significant findings, as detailed below:

1. The Pareto front analysis indicates that the low emission fluctuation conflict can provide an opportunity to more effectively balance the crucial cost vs. emission tradeoffs to achieve better solutions.

2. Energy savings measures for equipment, such as the dehumidification with heat recovery and hybrid welding, represent a considerable advantage in terms of both the economic and environmental viability of the microgrid.

The major contribution of the paper is providing a reference for the operation of energy management system in shipyards.

Future research may be useful to find new opportunities to further decrease the overall economic impact of the microgrid, using methods such as capacity optimization, policy incentives and technological advances.

References

[1] M. Xue, J. Xie, F. Chen, X. Ke, T. Xu, H. Hou, “Review on Multi-objective Joint Economic Dispatching of Microgrid in Power System”, Procedia Computer Science, vol. 130, 2018, pp. 1152–1157.

[2] Z. Li and Y. Xu, “Optimal coordinated energy dispatch of a multi-energy microgrid in grid-connected and islanded modes”, Applied Energy, vol. 210, Jan. 2018, pp. 974–986.

[3] Z. Guan, H. Wang, Z. Li, X. Luo, X. Yang, J. Fang, Q. Zhao, “Multi-Objective Optimal Scheduling of Microgrids Based on Improved Particle Swarm Algorithm”, Energies, vol. 17, no. 7, Apr. 2024, pp. 1760.

[4] X. Ma, Y. Mu, Y. Zhang, C. Zang, S. Li, X. Jiang, M. Cui, “Multi-objective microgrid optimal dispatching based on improved bird swarm algorithm”, Global Energy Interconnection, vol. 5, no. 2, Apr. 2022, pp. 154–167.

[5] T.-T. Nguyen, T.-G. Ngo, T.-K. Dao, T.-T.-T. Nguyen, “Microgrid Operations Planning Based on Improving the Flying Sparrow Search Algorithm”, Symmetry, vol. 14, no. 1, Jan. 2022, pp. 168.

[6] V. Tiwari, H. M. Dubey, M. Pandit, S. R. Salkuti, “Economic Dispatch in Microgrid with Battery Storage System using Wild Geese Algorithm”, Green Energy and Intelligent Transportation, Jan. 2025, pp. 100263.

[7] B. Dai, H. Wang, B. Li, C. Li, Z. Tan, “Capacity model and optimal scheduling strategy of multi-microgrid based on shared energy storage”, Energy, vol. 306, Oct. 2024, pp. 132472.

[8] Y.-L. He, X.-W. Wu, K. Sun, X.-Y. Liu, H.-P. Wang, S.-M. Zeng, Y. Zhang, “A Novel MOWSO algorithm for Microgrid multi-objective optimal dispatch”, Electric Power Systems Research, vol. 232, July 2024, pp. 110374.

[9] X. Wu, Y. Shan, K. Fan, “A Modified Particle Swarm Algorithm for the Multi-Objective Optimization of

Wind/Photovoltaic/Diesel/Storage Microgrids", Sustainability, vol. 16, no. 3, Jan. 2024, pp. 1065.
[10] X. Wang, Z. Li, X. Luo, Y. Zhang, X. Guan, "A Bi-level optimization dispatch for hybrid shipboard microgrid considering electricity-gas-heat coupling", Green Energy and Resources, vol. 2, no. 2, June 2024, pp. 100070.
[11] A. Ouammi, Y. Achour, H. Dagdougui, D. Zejli, "Optimal operation scheduling for a smart greenhouse integrated microgrid", Energy for Sustainable Development, vol. 58, Oct. 2020, pp. 129–137.
[12] M. Ghadi-sahebi and R. Ebrahimi, "Stochastic scenario based microgrid energy management with electric vehicles considering uncertainty sources", U.P.B. Sci. Bull., Series C, vol. 82, Iss. 1, 2020, pp. 259-276.
[13] F. Cheng, G. Shi, H. Lu, R. Gao, S. Yu, C. Song, J. Zhu, G. Xiao, K. Wu, "An example analysis of energy-saving improvement based on air compressor inlet pre-treatment", Journal of Physics: Conference Series, vol. 2674, no. 1, Dec. 2023, pp. 012016.
[14] Y. Hu, W. Xu, G. Jia, G. Li, M. Cai, "Energy Analysis of Precooling Air Compressor System", Entropy, vol. 24, no. 8, July 2022, pp. 1035.
[15] U. Hummel, P. Radgen, S. Ülker, R. Schelle, "Findings from Measurements of the Electric Power Demand of Air Compressors", Energies, vol. 14, no. 24, Dec. 2021, pp. 8395.
[16] L. Liu, C. Li, J. Shi, "Analysis of energy utilisation efficiency in laser–GTA hybrid welding process", Science and Technology of Welding and Joining, vol. 19, no. 7, Oct. 2014, pp. 541–546.
[17] A. Mahrle, S. Rose, M. Schnick, E. Beyer, U. Füssel, "Laser-assisted plasma arc welding of stainless steel", Journal of Laser Applications, vol. 25, no. 3, May 2013.
[18] L. Chen, S. H. Chen, L. Liu, B. Zhang, "Experimental investigation of precooling desiccant-wheel air-conditioning system in a high-temperature and high-humidity environment", International Journal of Refrigeration, vol. 95, Nov. 2018, pp. 83–92.
[19] R. S. Srivastava, A. Kumar, S. Sharma, H. Thakur, S. Patel, R. Vaish, "Development and applications of thermoelectric based dehumidifiers", Energy and Buildings, vol. 252, Dec. 2021, pp. 111446.
[20] Á. M. Costa, R. Bouzón, D. Vergara, J. A. Orosa, "Eco-friendly Pressure Drop Dehumidifier: An Experimental and Numerical Analysis", Sustainability, vol. 11, no. 7, Apr. 2019, pp. 2170.
[21] X. Qu, M. Zhao, Q. Qi, "Research on energy consumption evaluation and energy-saving design of cranes in service based on structure-mechanism coupling", Advances in Mechanical Engineering, vol. 16, no. 9, Sept. 2024.
[22] M. Kłodawski, R. Jachimowski, N. Chamier-Gliszczyński, "Analysis of the Overhead Crane Energy Consumption Using Different Container Loading Strategies in Urban Logistics Hubs", Energies, vol. 17, no. 5, Feb. 2024, pp. 985.
[23] S. Fei, G. Zhihao, T. Yifei, L. Xiangdong, "Characteristics analyses of energy consumption for bridge crane based on the energy flow", IOP Conf. Series: Materials Science and Engineering, vol. 758, no. 1, Feb. 2020, pp. 012002.
[24] L. C. R. Jones, N. Goffin, J. Ouyang, N. Mirhossein, J. Xiong, Y. Li, L. Li, J. Tyrer, Z. Liu, E. Woolley, Y. He, G. Mi, P. Mativenga, "Laser specific energy consumption: How do laser systems compare to other manufacturing processes?", Journal of Laser Applications, vol. 34, no. 4, Nov. 2022, pp. 042029.